ChemPubSoc Europe

DOI: 10.1002/cphc.201500682

CHEMPHYSCHEM Articles

On the Energetics of Ions in Carbon and Gold Nanotubes

Leila Mohammadzadeh,[a, b] Aleksej Goduljan,[a] Fernanda Juarez,[a] Paola Quaino,[b] Elizabeth Santos,[a, c] and Wolfgang Schmickler*[a]

We investigate the insertion of halide and alkali atoms into narrow single-walled carbon nanotubes with diameters <9 Å by density functional theory; both chiral and non-chiral tubes are considered. The atoms are stored in the form of ions; the concomitant charge transfer affects the band structure and makes originally semiconducting tubes conducting. The electrostatic interaction between a charge and the walls of the tube is explicitly calculated. The insertion energies and the positions of the ions are determined by a competition between electrostatic energy and Pauli repulsion. For comparison, we consider ions in gold nanotubes. Alkali ions follow the same principles in gold as in carbon tubes, but chloride is specifically adsorbed inside gold tubes.

1. Introduction

Nanotubes offer new opportunities to electrochemical technology. Because of their large surface area they are an excellent material for supercapacitors, and they also hold promises for lithium ion batteries and for electrocatalysis.[1–6] Therefore, there has been much research on ions in nanotubes, and the focus has usually been on lithium in carbon nanotubes (CNT) for obvious reasons. For electrochemistry the distribution of the charge is particularly important. For the case of lithium in CNT all theoretical studies agree that lithium intercalated in CNT transfers negative charge to the tube—for an early paper see Ref. [7]. Since CNTs typically have work functions of the order of 4.5–4.8 eV,[8] while the ionization energy of Li is about 5 eV, this indicates that the charge transfer is fostered by the interaction between the ion and the carbon tube; in a pristine carbon tube this interaction must be electrostatic, and is provided by the image interaction.[9] As we go down the column of the alkali metals, ionization energies become lower, and the driving force for a complete transfer of the valence electron to the carbon lattice increases.

Halide atoms inserted in small CNTs acquire a negative charge; their electron affinities lie in the range of 2.8–3.4 eV, and they require an even larger interaction to favor charge transfer. Nevertheless, we have recently found that at least in small CNTs, with diameters less than 1 nm, the halide ions are completely ionized.[10]

[a] L. Mohammadzadeh, A. Goduljan, Dr. F. Juarez, Dr. E. Santos, Prof. Dr. W. Schmickler
Institute of Theoretical Chemistry
Ulm University
89069 Ulm (Germany)

[b] L. Mohammadzadeh, Dr. P. Quaino
PRELINE, Universidad Nacional del Litoral
3000 Santa Fe (Argentina)

[c] Dr. E. Santos
Facultad de Matemática
Astronoma y Fsica, IFEG-CONICET
Universidad Nacional de Córdoba
5000 Córdoba (Argentina)

Another interesting point is the optimum position of ions within a nanotube. Recent models for the capacity of nanotubes filled with an ionic liquid assume that the ions are positioned at the center of the tube.[11–14] This is in line with an experimental study, where a one-dimensional chain of CsI was formed along the center of a small nanotube.[15] Our own group has investigated a series of alkali and halides in small gold and carbon nanotubes and found, that the ions were stable at the center of the tubes.[10] However, we also pointed out that this could not be true for wider tubes for rather obvious reasons. Indeed, several studies conducted for lithium, which is the smallest alkali ion, showed an equilibrium position for a lithium ion near the wall.[16–22] We shall focus on the role of the electrostatic interaction, which is assumed to play the dominant role in the above-mentioned models for the capacity, but shall also demonstrate, that this is balanced by Pauli repulsion. Finally, we note that doped CNTs are a special case, since doping breaks the symmetry and leads to an eccentric position of the lithium atom.[23]

In this article we want to investigate which interactions determine the positions and the insertion energies of the ions. For this purpose we investigated the energetics of alkali and halide ion insertion in various CNTs, and for comparison also in a few gold nanotubes (AuNTs), by DFT. In addition, we calculated the electrostatic interaction of point charges in conducting tubes in order to better understand the electrostatic part of the interaction.

2. Electrostatic Interactions

From our previous works we know that electrostatic interactions play a pivotal role, and we gave the expression for the image energy of a point charge situated at the center of a tube.[10] We now consider the more general case, a point charge situated at a distance ρ_0 from the center of a perfect metal tube with radius $R > \rho_0$. For a real system, the radius has to be replaced by the radius of the effective image cylinder, which we have defined in.[10] We shall return to this concept below.

The image interaction for the point charge with the wall can be calculated by the standard techniques of electrostatics; probably the problem has been solved before, but we have not been able to find a corresponding publication. Therefore, the derivation is given in the Computational Details section below. The image energy can be written in the form [Eq. (1)]:

$$V_{\mathrm{im}} = \frac{q}{R} f_{\mathrm{im}}(x_0) \tag{1}$$

where q is the charge and $x_0 = \rho_0/R$. The universal dimensionless function f_{im} is independent of the radius R and given by Equation (2):

$$f_{\mathrm{im}}(x_0) = -\frac{1}{\pi}\int_0^\infty dx \frac{I_0^2(xx_0)K_0(x)}{I_0(x)} - \frac{2}{\pi}\sum_{m=1}^{\infty}\int_0^\infty dx \frac{I_m^2(xx_0)K_m(x)}{I_m(x)} \tag{2}$$

where I_m and K_m denote Bessel functions in standard notation. It is displayed in Figure 1. It has a maximum for $x_0 = 0$, when the charge is right at the center. However, the maximum is very flat, the gradient vanishes at the center, and only for $x_0 > 0.5$ does the curve start to fall off noticeably. This means, that for a point charge the center of the tube is the least favorable position, and it is attracted to the wall. However, when it is placed right at the center, it will stay there because the slope is zero, and even a very small repulsive interaction from the wall will fix it in the center. Thus, Pauli repulsion is required to stabilize the ions inside the tubes.

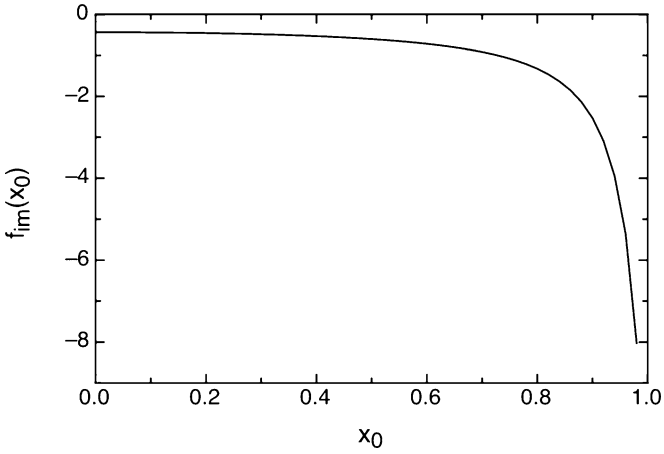

Figure 1. The universal dimensionless function $f_{\mathrm{im}}(x_0)$ that describes the image interactions; $x_0 = \rho_0/R$

3. Energetics of Simple Ions in Nanotubes

3.1. Details of the Investigated Systems

As in our previous publications,[9,10] we investigated atoms placed inside single-walled narrow carbon or gold nanotubes. While previously some CNTs had been represented by carbon rings, now all investigated tubes are infinite with appropriate periodic boundary conditions. A list is given in Table 1. Note that the (5,5)CNT and (6,3)CNT are conducting, while the (8,0)CNT and (6,2)CNT are semiconducting. The technical details of the DFT calculations are the same as in Ref. [10] and are given in the Computational Details section.

Table 1. Dimensions of the empty tubes. The length is that of the unit cell.

System	Diameter [Å]	Length [Å]
(5,5)CNT	6.78	12.82
(8,0)CNT	6.37	12.36
(6,3)CNT	6.21	11.35
(6,2)CNT	5.64	15.45
(6,6)AuNT	5.65	9.60
(8,8) AuNT	7.32	9.69
(12,6)AuNT	8.82	8.18

3.2. Effect of Ion Insertion on the Band Structure

The list of CNTs investigated comprises both conducting and semiconducting tubes. It is well known that the adsorption of lithium affects the band structure of CNTs[7] and of graphene:[24] lithium donates electrons, and makes the originally semiconducting structures conducting. For the concentration of lithium employed, we have observed the same effect for (8,0)CNT, which in the absence of ions is semiconducting—see lower panel in Figure 2. Insertion of Li donates an electron, the Fermi level is raised and is now occupied. The case of anionic insertion is especially interesting, since it has not been investigated so far. Adsorption of Cl causes the transfer of an electron from the CNT. Consequently the Fermi level is lowered, and is occupied—see middle panel in Figure 2. In addition, two occupied surface states are created, whose energies show no dispersion in k space.[25] These results should be compared with theoretical and experimental works,[26,27] which show an effect of halogen molecules on the electronic properties of CNTs.

3.3. Position of the Ions in the Tubes

As we have seen in the previous section, classical electrostatics favors a position of the ion away from the center. However, the center of the tube is always a stationary point for the electrostatic energy, so that in narrow tubes even a small repulsion will stabilize the ion in the center. Indeed, we shall see that for the tubes that we have investigated here the stable position is mostly at the center. As may be expected, the smallest ions investigated, Li^+ and Na^+, are off center in the widest tubes. In addition, we shall see that Cl adsorbs in AuNTs.

Figure 3 shows a few typical plots for the energy of the ions as a function of position; the energy at the center was set to zero. The top row shows the energy of Li^+ in Au(8,8)NT and (8,0)CNT. In both cases, the most stable position is away from the center. In the case of the AuNT, the difference in energy between the energies at the center and at the minimum is not large (about −0.1 eV) indicating that the repulsive potential from the gold walls is stronger than in the CNT. Since gold is

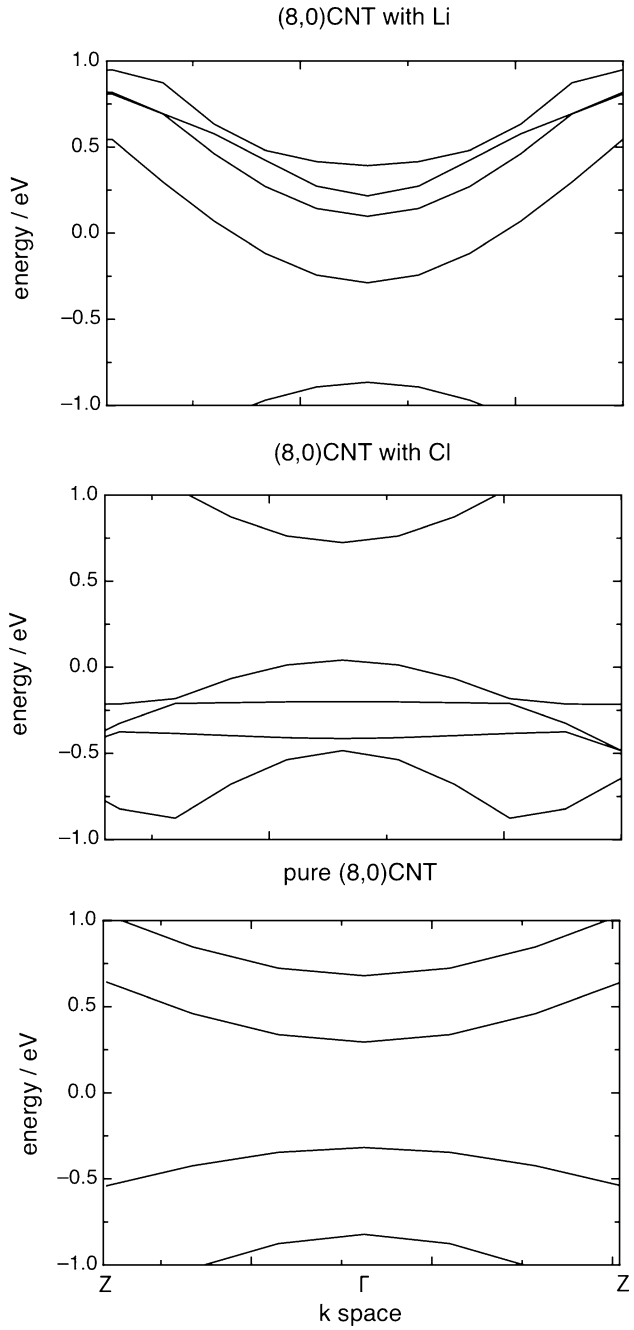

Figure 2. Band structure of the (8,0)CNT near the Fermi level, both in the presence and in the absence of ion insertion; the energy zero is at the Fermi level.

a metal, its electronic cloud is more extended, and hence Pauli repulsion is stronger. This is also the reason why the energy minimum is closer to the center than in the (8,0)CNT. In the latter, the Li^+ gains about 0.44 eV by moving from the center, and its stable position is closer to the wall. Also, there is a broad range of distances where the energy does not vary much. The results for Li^+ in (8,0)CNT are in general agreement with literature results.[16,17,22]

For the halide ions F^- and Cl^-, whose energies are shown in the bottom row, the minimum is at the center of the tube, because their radii are greater. Nevertheless, there is a certain range of distances, larger for F^- than for Cl^-, where the energy surface is rather flat.

While none of the ions investigated adsorb chemically on the CNTs, the halide ions can adsorb on the surface of the gold tubes. In particular, for Cl^- in (8,8)AuNT we found two locally stable positions: one at the center, and the other at the wall corresponding to a chemisorbed state, whose energy is about 0.7 eV lower than at the center. More details will be given below.

3.4. Insertion of Ions in Various Tubes

It is instructive to consider the energetics of ions in various tubes to elucidate the various contributions. We discuss anions and cations separately.

Anions in CNTs

From DFT we obtain the insertion energies of the atoms into the tubes through the relation [Eq. (3)]:

$$E_{ins} = E(\text{tube} + \text{ion}) - E(\text{tube}) - E(\text{atom}) \quad (3)$$

As discussed in Ref. [10] on insertion, the atoms attain a unit negative charge. Since this involves the transfer of an electron from the tube to the atom, we can decompose this into Equation (4):

$$E_{ins} = \Phi - E_A + E_{im} + E_{chem} \quad (4)$$

where Φ is the workfunction of the tube, E_A the electron affinity, E_{im} the image energy, and E_{chem} the chemical interaction, which in carbon nanotubes is mainly Pauli repulsion, since there is no evidence for chemical binding. The work function of the tube changes during electron transfer, so that we cannot simply use the work function of the isolated infinite tubes.[10] To compare the interaction of the ions with the tube, we eliminate the contribution of the electron affinity and define an ionic insertion energy as [Eq. (5)]:

$$E_{ins}^{ion} = E_{ins} + E_A \quad (5)$$

Since for a given tube the work function Φ does not depend on the inserted ion, variations of E_{ins}^{ion} between ions in the same tube can be attributed to the last two terms in Equation (4).

We have plotted the results in Figure 4 as a function of the radius of the tubes. As mentioned above, the stable position is always at the center of the tube. For the largest tube investigated, the smaller ions Cl^- and Br^- have practically the same insertion energy, indicating that the repulsion is small. The energy of the larger I^- is somewhat higher, indicating a noticeable effect of Pauli repulsion. This effect becomes stronger for the (8,0)CNT, where the insertion energy is different for the three ions and follows their size. For Cl^- and Br^- the energy is lower than in the (5,5) tube, since the image energy is lower

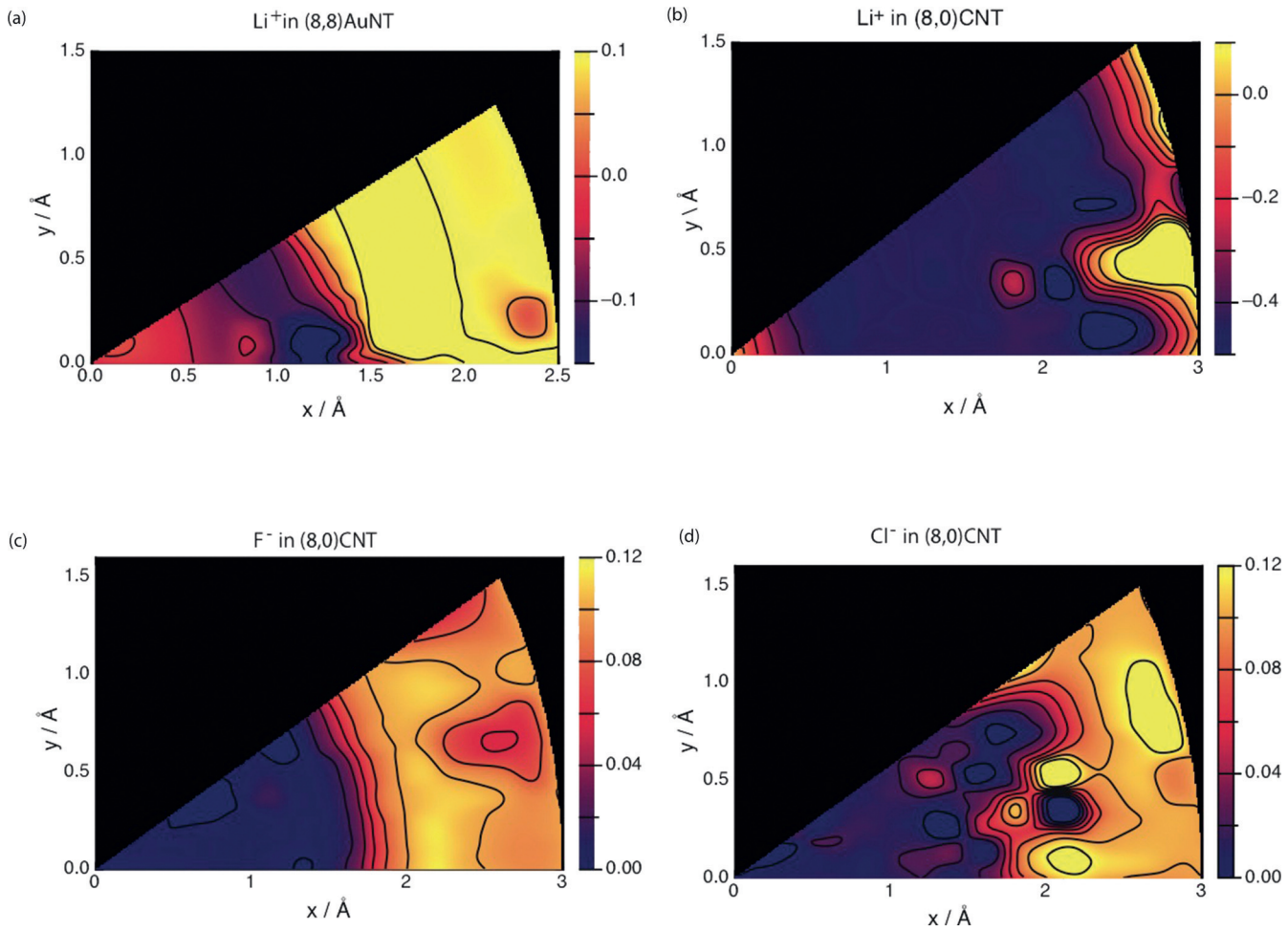

Figure 3. Examples for the energies of ions in nanotubes obtained by DFT as a function of position. The *z* coordinate is along the axis of the cylinder. In order to obtain a two-dimensional plot, we have chosen for each value of *x* and *y* the *z* coordinate where the energy is lowest, and plotted the corresponding energy as a function of *x* and *y*. Because of the symmetry, only a sector is displayed. The energy scales are in eV.

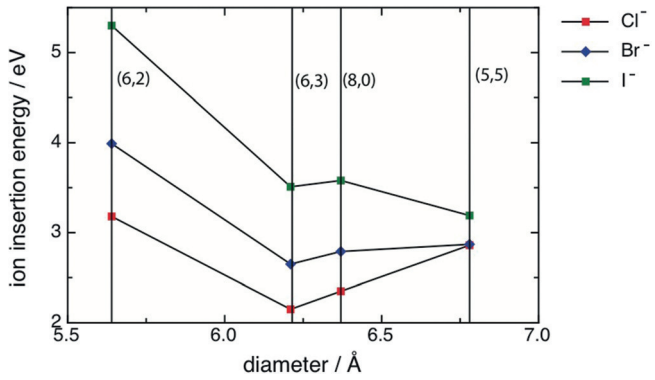

Figure 4. Insertion energy E_{ins}^{ion} of halide ions in various carbon nanotubes.

(more favorable); however, repulsion is somewhat greater for Br^-. For I^- the larger repulsion dominates over the gain in image energy. The insertion energies are lower for the slightly smaller (6,3) tube. Certainly the lower image energy plays a role, but the band structure could also have an effect: The (8,0)CNT is originally semiconducting, so that the electron is transferred from the valence band, which lies well below the Fermi level. Therefore the effective work function is higher, and the insertion energy in less favorable. In the narrow (6,2)CNT Pauli repulsion is large, and the insertion energies for the ions differ considerably in accord with their size.

Cations in CNTs

The alkali atoms lose an electron; therefore, instead of Equation (4) we now have Equation (6):

$$E_{ins} = -\Phi + I_1 + E_{im} + E_{chem} \quad (6)$$

where I_1 is the first ionization energy. Correspondingly, we define the ion insertion energy as [Eq. (7)]:

$$E_{ins}^{ion} = E_{ins} - I_1 \quad (7)$$

The corresponding results for Li^+ and Na^+ are shown in Figure 5. In the wide (5,5)CNT, both ions are off center; the smaller Li^+ ion is closer to the wall and has hence a substantially lower energy, since the image energy becomes more favorable with decreasing distance. The adsorption energies are even

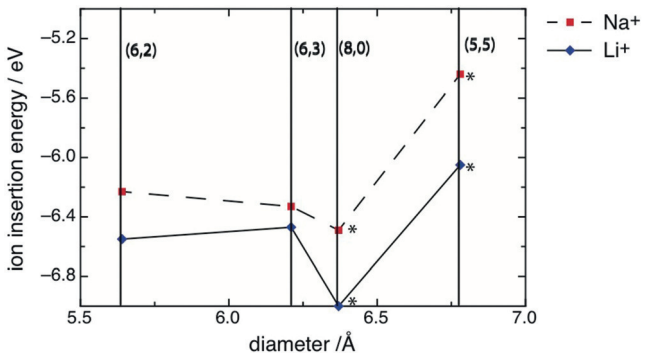

Figure 5. Insertion energy E_{ins}^{ion} of alkali ions in various carbon nanotubes. Values marked with an asterisk refer to adsorption sites off the axis.

lower for the smaller (8,0)CNT, since the larger curvature causes a more favorable image energy. For even smaller radii repulsion starts to play a role. Note that the variation of the insertion energy for Li^+ and Na^+ is much smaller than for the halide ions (see Figure 4).

Screening of the Coulomb Potential along the Axis

The formation of the image charge screens the Coulomb potential along the axis. In a previous publication,[10] we introduced a quantitative description for this effect: the effective image radius R_{im} of the tube. This is the radius of a classical metal tube which would screen the Coulomb potential of an ion at the center in the same way. We had calculated this radius for a series of carbon *rings*. Here we want to examine, if the screening effect is different for infinite carbon *tubes*, and if there is a major difference between conducting and semiconducting carbon tubes. For this purpose we have examined the screening of the Coulomb potential along the axis for a Li^+ ion at the center of a (8,0)CNT and a (5,5)CNT. Both have similar radii (3.18 Å and 3.10 Å, resp.), but the former is semiconducting, the latter metallic.

The screened Coulomb potentials are shown in Figure 6; they appear very similar. An evaluation of the effective image radius gives $R_{im} = 2.14$ Å for the (8,0)CNT, and $R_{im} = 2.01$ Å for the (5,5)CNT. Thus the difference between physical radius and the image radius is practically the same for both tubes. This is caused by the fact that the semiconducting tube is made conducting by the transfer of an electron from Li. Also, the image radius for the infinite (8,0)CNT and the corresponding ring, for which we had obtained $R_{im} = 1.90$ Å are very similar.

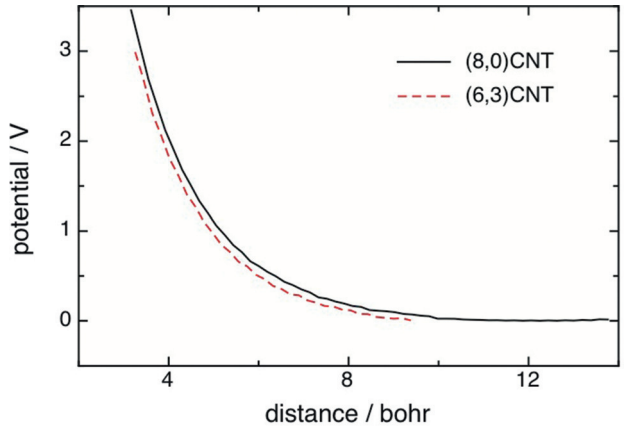

Figure 6. Screened Coulomb potential along the axis of a (8,0)CNT and a (5,5)CNT; the Li^+ ion sits at the origin at the center of the tube.

Ions in Gold Nanotubes

The graphite tubes show no proper chemical interactions with the investigated ions. In contrast, the gold atoms chemisorb chloride ions; in addition, they are much larger than the carbon atoms, and their electrons more mobile, so that they screen the ionic charge more effectively. We have collected a few representative results in Table 2.

Table 2. Insertion energies of ions in various gold nanotubes; *d* is the diameter of the tube; opt. denotes the optimum position of the ion.

Nanotube	Ion	*d* [Å]	E_{ins}^{ion} [eV]
(6,6)AuNT	Cs^+	5.65	−3.99
(6,6)AuNT	Na^+	5.65	−8.04
(6,6)AuNT	Li^+	5.65	−7.80
(8,8)AuNT	Li^+ opt.	7.12	−8.03
(8,8)AuNT	Li^+ center	7.12	−7.90
(12,6) AuNT	Li^+ opt.	8.82	−8.30
(12,6) AuNT	Li^+ center	8.82	−7.52
(8,8)AuNT	Cl^- opt.	7.12	2.15
(8,8)AuNT	Cl^- center	7.12	2.84

The (6,6)AuNT is so small that the stable position of the investigated ions is at the center. Li^+ and Na^+ have very similar insertion energies, so that they are governed by the image energy. Cs^+ is too thick and experiences a significant repulsion. In the (8,8)AuNT the stable position is off center (see also Figure 3), but the ions are also locally stable at the center, and the difference in energy between the two positions is small; the two positions are separated by an energy barrier of about 0.1 eV. In the larger (12,6)AuNT the difference in energy between the ion at the center and at the optimum position is much larger; in view of the large difference in image energy,—see Figure 1—this is not surprising.

Chlorine is chemisorbed in (8,8)AuNTs; the bond is polar, with an excess of electrons on the Cl (Bader charge −0.4). The difference in energy between the position at the center and the adsorption site is about 0.7 eV. This strong bond weakens the gold-gold interaction and leads to a small deformation of the gold tube (see Figure 7). This is reminiscent of the enhancement of gold adatom diffusion by adsorbed chlorine,[28] which is also caused by the weakening of the gold-gold interaction.

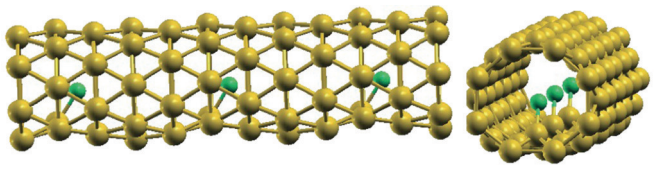

Figure 7. Two views of a chlorine atom adsorbed in (8,8)AuNT. Note the deformation of the gold lattice.

4. Conclusions

In this work, we have investigated the insertion of a variety of alkali and halogen atoms into narrow single-walled CNTs. On insertion, the atoms were fully ionized. The charge exchange with the CNTS affects the band structure, and turns those tubes that were originally semiconductors into conductors. None of the ions is adsorbed chemically; their position inside the tube and their energies of adsorption are determined by a competition between electrostatic image interactions, which favor a position at the wall, and Pauli repulsion. In models for charge storage it is often assumed that in small tubes the ions are at the center, but we have found several cases where small alkali ions are positioned near the wall, in agreement with previous reports on DFT calculations for lithium ions in CNTs.

Following up on our previous work,[9,10] we have also investigated the screening of the Coulomb potential along the axis of the tube. In particular we wanted to see if there is a difference between semiconducting and conducting CNTs. Within the accuracy of our calculations we found no difference in the screening, because the charge transfer has made the non-chiral tubes conducting.

For comparison, we have also performed calculations for these ions in gold NTs. The insertion of alkali ions is governed by the same principles as in CNTs, but Pauli repulsion is stronger since the electronic cloud is more extended. Chlorine, however, is specifically adsorbed; the bond is polar with an excess of electrons on the Cl atom, and induces a deformation of the tube.

In summary, we believe that we have made a significant step in understanding the behaviour of simple ions in nanotubes, and are now ready to tackle more complicated systems involving several ions and solvent in order to understand the double layer in narrow tubes.

Computational Details

Image Potential of a Point Charge in a Conducting Cylinder

We consider a conducting cylinder of radius R, whose axis coincides with the z axis of the coordinate system (see Figure 8). Throughout this section, we shall employ cylindrical coordinates (ρ, ϕ, z) with the usual meaning, and use Jackson[29] as our standard reference. Let the point charge be situated at $(\rho_0, 0, 0)$; it gives rise to the usual Coulomb potential $\Psi(\rho, \phi, z)$, and in addition generates an image charge, which in turn generates an image potential $\Psi_{\text{im}}(\rho, \phi, z)$. In order to calculate the image energy, we need the value of the image potential at the position of the point charge. Inside the cylinder, the image potential satisfies Laplace's equation; on the surface of the cylinder, it must cancel the potential generated by the point charge.

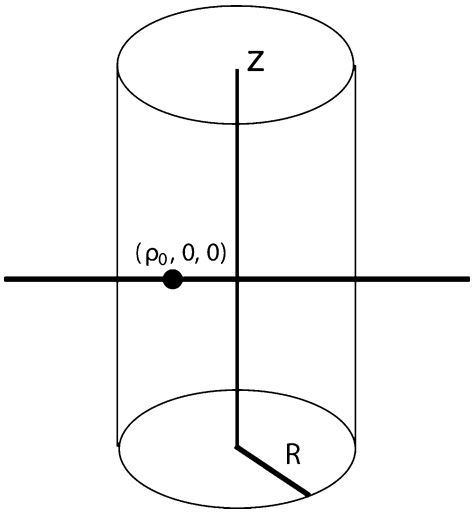

Figure 8. Conducting cylinder with point charge.

Using a standard expansion of the Coulomb potential, we can write the potential of the point charge taken at the surface of the cylinder as [Eq. (8)]:

$$\Psi(R,\phi,z) = \frac{4}{\pi}\int_0^\infty dk\cos(kz) \times\left\{\frac{1}{2}I_0(k\rho_0)K_0(kR) + \sum_{m=1}^{\infty}\cos(m\phi)I_m(k\rho_0)K_m(kR)\right\} \tag{8}$$

Inside the tube, the potential generated by the image charge obeys Laplace's equation and can be written in the general form [Eq. (9)]:

$$\Psi_{\text{im}}(\rho,\phi,z) = \sum_{m=0}^{\infty}\int_0^\infty dk\cos(kz)I_m(k\rho)[A_m(k)\sin(m\phi) + B_m(k)\cos(m\phi)] \tag{9}$$

where the functions I_m and K_m denote the appropriate Bessel functions in standard notation. To determine the unknown coefficients $A_m(k)$ and $B_m(k)$, we take the value on the surface of the cylinder, which must cancel $\Psi(R, \phi, z)$, as given by Equation (8):

$$\Psi_{\text{im}}(R,\phi,z) = \sum_{m=0}^{\infty}\int_0^\infty dk\cos(kz)I_m(kR)[A_m(k)\sin(m\phi) + B_m(k)\cos(m\phi)] \tag{10}$$

Comparison with Equation (8) gives [Eq. (9)]:

$$A_m(k) = 0$$
$$B_0(k) = -\frac{2}{\pi}\frac{I_0(k\rho_0)K_0(kR)}{I_0(kR} \tag{11}$$
$$B_m(k) = -\frac{4}{\pi}\frac{I_m(k\rho_0)K_m(kR)}{I_m(kR)} \quad for \quad m\neq 0$$

If in Equation (8) we substitute R by the general cylindrical radius ρ, we obtain the direct Coulomb potential of the point charge in cylindrical coordinates. If we combine this with Equations (10) and

(11), we obtain the total electrostatic potential at any point inside the tube.

For our purposes, we need the image potential at the point $(\rho_0, 0, 0)$ of the point charge [Eq. (12)]:

$$\Psi_{\text{im}}(\rho_0, 0, 0) = \sum_{m=0}^{\infty} \int_0^{\infty} dk I_m(k\rho_0) B_m(k) \tag{12}$$

With the substitution $x = kR$ and $x_0 = \rho_0/R$ we obtain Equations (13) and (14):

$$\Psi_{\text{im}}(\rho_0, 0, 0) = -\frac{2}{\pi R} \int_0^{\infty} dx \frac{I_0^2(xx_0) K_0(x)}{I_0(x)} \tag{13}$$

$$-\frac{4}{\pi R} \sum_{m=1}^{\infty} \int_0^{\infty} dx \frac{I_m^2(xx_0) K_m(x)}{I_m(x)} \tag{14}$$

The image energy is $V_{\text{im}} = q\Psi_{\text{im}}(\rho_0, 0, 0)/2$. Note that it can be written in the form [Eq. (15)]:

$$V_{\text{im}} = \frac{q}{R} f_{\text{im}}(x_0) \tag{15}$$

where $f_{\text{im}}(x_0)$ is a universal function, independent of the radius R of the tube. It is displayed in Figure 1.

For large radii R of the tube, the image law must converge to the image law for a plane surface, which is $-q/4a$, where $a = R - \rho_0$ is the distance from the surface. In terms of our notation this means [Eq. (16)]:

$$\lim_{R\to\infty} -\frac{a}{R} f_{\text{im}}(1 - a/R) = \frac{1}{4} \tag{16}$$

We have not been able to find a general proof, but to check the numerical accuracy of our program we have calculated $g_{\text{im}} = -\frac{a}{R} f_{\text{im}}(1 - a/R)$ as a function of a/R; Figure 9 shows that it converges indeed to $1/4$. The larger the value of R, the more terms of the sum over m must be retained.

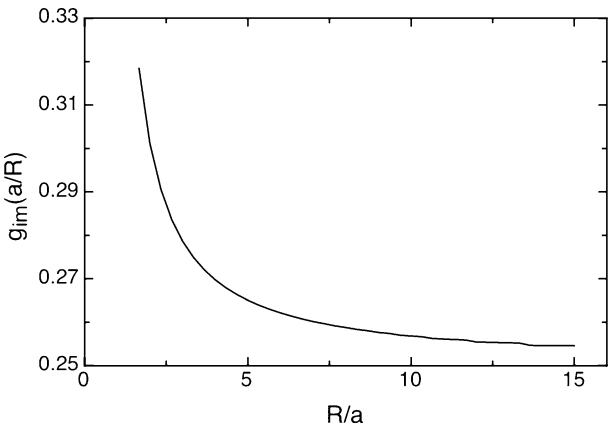

Figure 9. Asymptotic behavior for large R: g_{im} as a function of R/a; at large values the function tends towards $1/4$, which is the value for a flat surface.

Technical Details of the DFT Calculation

We studied alkali and halide atoms placed inside of single-walled carbon and gold nanotubes by performing density functional theory (DFT) calculations. The correlation and exchange functionals were described within the generalized gradient approximation (GGA) in the Perdew, Burke and Ernzerhof (PBE) flavor.[30] The electron-ion interactions were represented through ultrasoft pseudopotentials[31] and a plane wave basis set was used to describe the valence electrons. The basis set was expanded to a kinetic energy cutoff of 400 eV (450 eV for the density). Brilloun zone integration was performed using the Gamma point. The carbon and gold nanotubes were studied by using VASP[32] and DACAPO[33] codes, respectively. Periodic boundary conditions were used in order to correctly represent the infinite nanotubes. A separation of 15 Å between neighbor systems was imposed in the directions perpendicular to the tubes and in order to avoid interactions between neighbor images. All the nanotubes and alkali or halide atoms were fully relaxed until the total forces were less than 40 meVA^{-1}. All the systems used were neutral, but we confirmed the loss or gain of charge in the central atom by using Bader analysis method.[34] We used a dipole-correction scheme[35] in the systems that are not completely symmetric, in order to have a well-defined vacuum potential. The electrostatic part (ionic and Hartree potentials) of the local potential was calculated, but the exchange-correlation was not added.

Acknowledgements

We thank Prof. Dr. A. Kornyshev from Imperial College, London, for very useful discussions. Financial supports by the Deutsche Forschungsgemeinschaft (FOR 1376), and by an exchange agreement between the DAAD-Mincyt are gratefully acknowledged. P.Q., E.S. and W.S. thank CONICET for continued support. E. S. acknowledges PIP-CONICET 112-2010001-00411, and PICT- 2012-2324 (Agencia Nacional de Promoci—n Cient'fica y Tecnol—gica, FONCYT, pržstamo BID) for support, while P.Q. thanks CAID 501 201101 00276 LI UNL for support. A generous grant of computing time from the Baden-WŸrttemberg grid is gratefully acknowledged.

Keywords: carbon nanotubes · density functional theory · halides · ion storage · screening

[1] F. Leroux, K. Metenier, S. Gautier, E. Frackowiak, S. Bonnamy, F. Beguin, *J. Power Sources* **1999**, *81*, 317.
[2] G. T. Wu, C. S. Wang, X. B. Zhang, H. S. Yang, Z. F. Qi, P. M. He, W. Z. Li, *J. Electrochem. Soc.* **1999**, *146*, 1696.
[3] E. Frackowiak, S. Gautier, H. Gaucher, S. Bonnamy, F. Beguin, *Carbon* **1999**, *37*, 61.
[4] C. Niu, E. K. Sichel, R. Hoch, D. Moy, H. Tennent, *Appl. Phys. Lett.* **1997**, *70*, 1480.
[5] L. Diederich, E. Barborini, P. Piseri, A. Podesta, P. Mi-lani, A. Schneuwly, R. Gallay, *Appl. Phys. Lett.* **1999**, *75*, 2662.
[6] R. Z. Ma, J. Liang, B. Q. Wei, B. Zhang, C. L. Xu, D. H. Wu, *J. Power sources* **1999**, *84*, 126.
[7] J. Zhao, A. Buldum, J. Han, J. P. Lu, *Phys. Rev. Lett.* **2000**, *85*, 1706.
[8] W. S. Su, T. C. Leung, C. T. Chan, *Phys. Rev. B* **2007**, *76*, 235413.
[9] A. Goduljan, F. Juarez, L. Mohammadzadeh, P. Quaino, E. Santos, W. Schmickler, *Electrochem. Commun.* **2014**, *45*, 48.
[10] L. Mohammadzadeh, A. Godolijan, F. Juarez, P. Quaino, E. Santos, W. Schmickler, *Electrochim. Acta* **2015**, *162*, 11.
[11] S. Kondrat, A. Kornyshev, *J. Phys. Condens. Matter* **2011**, *23*, 022201.
[12] C. Rochester, A. Lee, G. Pruessner, A. Kornyshev, *ChemPhysChem* **2013**, *14*, 4121.
[13] A. Lee, S. Kondrat, A. Kornyshev, *Phys. Rev. Lett.* **2014**, *113*, 048701.
[14] A. Kornyshev, *Faraday Discuss.* **2013**, *164*, 117.

[15] R. Senga, K. Hannu-Pekka, Z. Liu, K. Hirose-Takai, A. V. Krasheninnikov, K. Suenaga, *Nat. Mater.* **2014**, *13*, 1050.
[16] T. Kar, J. Pattanayak, S. Scheiner, *J. Phys. Chem. A* **2001**, *105*, 10397.
[17] A. Udomvech, T. Kerdcharoen, T. Osotchan, *Chem. Phys. Lett.* **2005**, *406*, 161.
[18] Z. Zhou, J. Zhao, X. Gao, Z. Chen, J. Yan, P. von Rague Schleyer, M. Morinaga, *Chem. Mater.* **2005**, *17*, 992.
[19] V. Meunier, J. Kephart, C. Roland, J. Bernholc, *Phys. Rev. Lett.* **2002**, *88*, 075506.
[20] E. Durgun, S. Dag, V. Bagci, O. Gülseren, T. Yildrim, S. Ciraci, *Phys. Rev. B* **2003**, *67*, 201401.
[21] M. Kantha, N. Cordero, J. Alonso, M. Cawkwell, L. Girifolco, *Phys. Rev. B* **2008**, *78*, 115430.
[22] O. M. Korsun, O. N. Kalugin, O. V. Prezhdo, *J. Phys. Chem. Lett.* **2014**, *5*, 4129.
[23] D. Quiñonero, A. Frontera, C. Garau, A. Costa, P. Ballester, P. M. Deya, *Chem. Phys. Lett.* **2005**, *411*, 256.
[24] Y. Liu, M. Wang, B. Yakobson, B. C. Wood, *Phys. Rev. Lett.* **2014**, *113*, 028304.
[25] A. Groß, *Theoretical Surface Science* Springer Verlag, **2003**, p. 61ff.
[26] S. Gosh, S. Yamijala, S. Pati, C. Rao, *RSC Adv.* **2012**, *2*, 1181.
[27] T. Liang, W.-X. Li, H. Zhang, *J. Mol. Struct.* **2000**, *905*, 44.
[28] M. Mesgar, P. Kaghazchi, T. Jacob, E. Pichardo-Pedrero, M. Giesen, H. Ibach, N. B. Luque, W. Schmickler, *ChemPhysChem* **2013**, *14*, 233.
[29] D. Jackson, *Classical Electrodynamics*, John Wiley & Sons, New York, **1962**.
[30] J. P. Perdew, K. Burke, M. Ernzerhof, *Phys. Rev. Lett.* **1996**, *77*, 3865.
[31] D. Vanderbilt, *Phys. Rev. B* **1990**, *41*, 7892.
[32] a) G. Kresse, J. Hafner, *Phys. Rev. B* **1993**, *47*, 558; b) G. Kresse, J. Hafner, *Phys. Rev. B* **1994**, *49*, 14251.
[33] B. Hammer, L. B. Hansen, J. K. Nørskov, *Phys. Rev. B* **1999**, *59*, 7413.
[34] a) R. F. W. Bader, P. E. Cade, P. M. Beddall, *J. Am. Chem. Soc.* **1971**, *93*, 3095; b) G. Henkelman, A. Arnaldsson, H. Jonsson, *Comput. Mater. Sci.* **2006**, *36*, 354.
[35] L. Bengtsson, *Phys. Rev. B* **1999**, *59*, 12301.

Manuscript received: August 14, 2015
Revised: October 23, 2015
Accepted Article published: October 27, 2015
Final Article published: November 13, 2015